



CHORUS

This is the accepted manuscript made available via CHORUS. The article has been published as:

Spontaneous decay of a quantum emitter near a plasmonic nanostructure

Tigran V. Shahbazyan

Phys. Rev. B **98**, 115401 — Published 4 September 2018

DOI: [10.1103/PhysRevB.98.115401](https://doi.org/10.1103/PhysRevB.98.115401)

Spontaneous decay of a quantum emitter near a plasmonic nanostructure

Tigran V. Shahbazyan

Department of Physics, Jackson State University, Jackson, MS 39217 USA

We develop a theory for spontaneous decay of a quantum emitter (QE) situated near metal-dielectric structure supporting localized surface plasmons. If plasmon resonance is tuned close to the QE emission frequency, the emission is enhanced due to energy transfer from QE to localized plasmon mode followed by photon emission by plasmonic antenna. The emission rate is determined by intimate interplay between the plasmon coupling to radiation field and the Ohmic losses in metal. Here we develop plasmon Green function approach that includes plasmon's interaction with radiation to obtain explicit expressions for radiative decay rate and optical polarizability of a localized plasmon mode in arbitrary plasmonic nanostructure. Within this approach, we provide consistent definition of plasmon mode volume by relating it to plasmon mode density, which characterizes the plasmon field confinement, and recover the standard cavity form of the Purcell factor, but now for plasmonic systems. We show that, for QE placed at "hot spot" near sharp tip of a small metal nanostructure, the plasmon mode volume scales with the metal volume while being very sensitive to the proximity to the tip. Finally, we derive the enhancement factor for radiated power spectrum for any nanoplasmonic system and relate it to the Purcell factor for spontaneous decay rate. We illustrate our results by numerical example of a QE situated near gold nanorod tip.

I. INTRODUCTION

Rapid advances in nanoplasmonics during past decade opened up avenues for extremely high energy concentration and transfer on length scale well below the diffraction limit [1–3]. Optical interactions between dye molecules or semiconductor quantum dots, hereafter referred to as quantum emitters (QEs), and localized plasmons in metal-dielectric structures underpin major phenomena in plasmon-enhanced spectroscopy such as surface-enhanced Raman scattering (SERS) [4], plasmon-enhanced fluorescence and luminescence [5–11], strong QE-plasmon coupling [12–23], and plasmonic laser [24–26]. On theory side, however, despite significant progress in various aspects of plasmonics, a consistent description of spontaneous decay of a QE near plasmonic nanostructure characterized by dispersive and lossy dielectric function is still a subject of active debate [27–36].

Spontaneous decay of a QE near photonic or plasmonic resonator can be strongly modified due to additional energy transfer (ET) channel provided by the QE coupling to cavity or plasmonic modes [37]. If the mode frequency ω_m is tuned close to the QE emission frequency, the QE decay rate can be greatly enhanced relative to free-space decay rate γ_0^r . The modified rate is usually presented as $\gamma = \gamma_0^r + \gamma_{et} = \gamma_0^r (1 + F_p)$, where γ_{et} is ET rate between QE and resonant mode whereas F_p is the Purcell factor characterizing the decay rate enhancement [38]. For QE coupled to cavity mode, the Purcell factor has the form

$$F_p = \frac{\gamma_{et}}{\gamma_0^r} = \frac{6\pi Q_m}{k^3 \mathcal{V}_m}, \quad (1)$$

where Q_m is the mode quality factor, \mathcal{V}_m is the mode volume and $k = \omega/c$ is the light wave vector (ω and c are frequency and speed of light). For photonic cavities, the mode volume at some point \mathbf{r} is defined as $\mathcal{V}_{cav} = \int dV \varepsilon(\mathbf{r}) |\mathbf{E}_m(\mathbf{r})|^2 / [\varepsilon(\mathbf{r}) |\mathbf{E}_m(\mathbf{r})|^2]$, where $\mathbf{E}_m(\mathbf{r})$ is the mode electric field and $\varepsilon(\mathbf{r})$ is (lossless) dielectric

function, and is usually interpreted as the volume that would confine the mode at given field intensity.

Spontaneous decay of a QE coupled to *plasmonic* resonator has been addressed within several approaches [29–36] aiming to obtain the corresponding Purcell factor in the form (1). While the plasmon quality factor is well defined as $Q_m = \omega_m / \gamma_m$, where γ_m is the plasmon decay rate, there has been active debate as to how unambiguously define the plasmon mode volume for QE located outside a metal nanostructure characterized by complex dispersive dielectric function [36, 39–49]. For open systems, straightforward analogies with photonic cavities do not apply and more rigorous, albeit less intuitive, numerical methods based on modal expansion of Maxwell equations' solutions are often employed [44, 49].

Here we develop another approach more suitable for nanoplasmonic systems which extends the quasistatic approximation, valid for system scale below the diffraction limit, to incorporate the plasmon coupling to radiation field in a consistent way. Specifically, if the system size L is much smaller than the photon wavelength λ then, on the far field scale $r \gg \lambda$, interaction of localized plasmon mode with radiation field is analogous to that of a point-like emitter with dipole moment $\mathcal{P}_m = \int dV \mathbf{P}_m$, where $\mathbf{P}_m(\mathbf{r})$ is the electric polarization vector of plasmon mode. On the other hand, on the near field scale $L \ll \lambda$, QE decay involves ET to plasmon at a rate γ_{et} determined by the plasmon local density of states (LDOS) [50]. Subsequently, some part of transferred energy is radiated away by the plasmonic antenna while the rest is dissipated in metal due to the Ohmic losses. An accurate treatment of spontaneous decay requires matching the balance between transferred and dissipated energy in the near field to the radiated energy in the far field. As we show in this paper, this is accomplished by including the plasmon coupling to radiation field into the plasmon Green function, which defines the LDOS, in a way that ensures energy flux conservation across the scales.

In the preceding paper [50], we derived the plasmon Green function for arbitrary metal-dielectric system with Ohmic losses included, but *without* coupling to the radiation field, in order to describe plasmonic enhancement of Forster ET between donors and acceptors. In this paper, we extend our approach to include the plasmon coupling to radiation field, and derive explicit expression for the plasmon radiative decay rate γ_m^r . By incorporating γ_m^r into the plasmon Green function, we obtain optical polarizability of plasmonic system describing its response to an external field in the way that satisfies energy flux conservation. We then turn to spontaneous decay of a QE coupled to plasmonic resonator and derive the Purcell factor for decay rate in the form (1), where the mode volume is identified as the inverse of plasmon mode density that characterizes plasmon field confinement at the QE position. We show that near sharp tip of small metal nanostructure, where the plasmon field is strongly confined (hot spot), the mode volume scales with the metal volume but, at the same time, is very sensitive to the QE distance to metallic tip. Finally, we derive enhancement factor for radiated power spectrum, which describes, e.g., plasmonic enhancement of fluorescence near metal nanostructures [5–11], and establish general relation between the enhancement and Purcell factors.

The paper is organized as follows. In Sec. II we revisit our derivation of the plasmon Green function [50] by using different method that makes its generalization more convenient. In Sec. III, we extend this approach by including the plasmon coupling to radiation field into Green function, and derive explicit expressions for radiative decay rate and optical polarization of any nanoplasmonic system. In Sec. IV, we derive the plasmon LDOS, plasmon mode density, and plasmon mode volume, as well as evaluate the plasmon mode volume near sharp tip of metal nanostructure. In Sec. V, we derive the Purcell factor for spontaneous decay of a QE coupled to plasmonic resonator and obtain explicit expression for the power spectrum enhancement factor. In Sec. VI, we illustrate our results numerically for a QE situated near the tip of Au nanorod. A summary of our results is provided in Sec. VII, and some details of our calculations are outlined in the Appendix.

II. SPONTANEOUS DECAY AND PLASMON GREEN FUNCTION

Consider an excited QE with dipole matrix element and orientation μ and \mathbf{n} , respectively, located at some position \mathbf{r} near metal-dielectric structure described by complex dielectric function $\varepsilon(\omega, \mathbf{r}) = \varepsilon'(\omega, \mathbf{r}) + i\varepsilon''(\omega, \mathbf{r})$ and surrounded by homogeneous medium with dielectric constant ε_s . We set $\varepsilon_s = 1$ for now, but will restore it when discussing numerical examples. The full decay rate of a QE in electromagnetic environment has the form [37]

$$\gamma = \frac{8\pi\omega^2\mu^2}{c^2\hbar} \text{Im} [\mathbf{n} \cdot \bar{\mathbf{G}}(\omega; \mathbf{r}, \mathbf{r}) \cdot \mathbf{n}], \quad (2)$$

where $\bar{\mathbf{G}}(\omega; \mathbf{r}, \mathbf{r}')$ is the dyadic Green dyadic for Maxwell equation satisfying $\nabla \times \nabla \times \bar{\mathbf{G}} - (\omega^2/c^2)\varepsilon \bar{\mathbf{G}} = \mathbf{I}$. For a QE in free space, the decay rate is determined by imaginary part of free-space Green function $\bar{\mathbf{G}}_0(\omega; \mathbf{r}, \mathbf{r}')$ at the QE position, $\text{Im}[\bar{\mathbf{G}}_0(\omega; \mathbf{r}, \mathbf{r})] = (\omega/6\pi c)\mathbf{I}$, yielding

$$\gamma_0^r = \frac{4\mu^2\omega^3}{3\hbar c^3}. \quad (3)$$

For systems with characteristic size below the diffraction limit, it is convenient to use rescaled Green function,

$$\bar{\mathbf{D}}(\omega; \mathbf{r}, \mathbf{r}') = \frac{4\pi\omega^2}{c^2} \bar{\mathbf{G}}(\omega; \mathbf{r}, \mathbf{r}'), \quad (4)$$

which, in the *near-field* limit, represents the sum of direct and plasmon terms, $\bar{\mathbf{D}} = \bar{\mathbf{D}}_0 + \bar{\mathbf{D}}_{\text{pl}}$ [50]. The full decay rate (2) takes the form $\gamma = \gamma_0^r + \gamma_{et}$, where

$$\gamma_{et} = \frac{2\mu^2}{\hbar} \text{Im} [\mathbf{n} \cdot \bar{\mathbf{D}}_{\text{pl}}(\omega; \mathbf{r}, \mathbf{r}) \cdot \mathbf{n}] \quad (5)$$

is QE-plasmon ET rate.

A. Plasmon Green function: lossless case

For metal-dielectric system with characteristic size smaller than the radiation wavelength, the fields and frequencies of plasmon modes are determined by quasistatic Gauss law [3]

$$\nabla \cdot [\varepsilon'(\omega_m, \mathbf{r}) \nabla \Phi_m(\mathbf{r})] = 0, \quad (6)$$

where the potentials $\Phi_m(\mathbf{r})$, which define the mode electric fields as $\mathbf{E}_m(\mathbf{r}) = -\nabla \Phi_m(\mathbf{r})$, satisfy the standard boundary conditions across metal-dielectric interfaces. The mode fields, which we chose to be real, are orthogonal, $\int dV \mathbf{E}_m(\mathbf{r}) \cdot \mathbf{E}_n(\mathbf{r}) = \delta_{mn} \int dV E_m^2(\mathbf{r})$, and regular inside the structure while falling off rapidly outside it.

In our preceding paper [50], the plasmon Green function in the presence of Ohmic losses was derived by expressing it through complex eigenvalues of operator $\nabla \cdot [\varepsilon(\omega, \mathbf{r}) \nabla]$. In this section, we give a more transparent derivation without resorting to eigenvalue problem, which permits its generalization to include, in the next section, the plasmon coupling to radiation field.

The Green function $S(\omega; \mathbf{r}, \mathbf{r}')$ for quasistatic potentials satisfies equation

$$\nabla \cdot [\varepsilon(\omega, \mathbf{r}) \nabla S(\omega; \mathbf{r}, \mathbf{r}')] = 4\pi\delta(\mathbf{r} - \mathbf{r}'), \quad (7)$$

for arbitrary frequency ω . In free space ($\varepsilon = 1$), the quasistatic Green function is independent of frequency and has the form $S_0(\mathbf{r} - \mathbf{r}') = -1/|\mathbf{r} - \mathbf{r}'|$; the corresponding dyadic Green function for fields, given by $\nabla \nabla' S_0(\mathbf{r} - \mathbf{r}')$, coincides with (real part of) free-space electromagnetic Green function (4) in the near-field limit. After splitting S into free-space and plasmon parts, $S = S_0 + S_{\text{pl}}$, we obtain equation for S_{pl} :

$$\begin{aligned} \nabla \cdot [\varepsilon(\omega, \mathbf{r}) \nabla S_{\text{pl}}(\omega; \mathbf{r}, \mathbf{r}')] \\ = -\nabla \cdot [[\varepsilon(\omega, \mathbf{r}) - 1] \nabla S_0(\omega; \mathbf{r}, \mathbf{r}')]. \end{aligned} \quad (8)$$

Assume, for a moment, that dielectric function $\varepsilon(\omega, \mathbf{r})$ is lossless ($\varepsilon'' = 0$). For real ε , the Green function can be expanded in terms of eigenmodes of Eq. (6) as

$$S_{\text{pl}}(\omega; \mathbf{r}, \mathbf{r}') = \sum_m S_m(\omega) \Phi_m(\mathbf{r}) \Phi_m(\mathbf{r}'), \quad (9)$$

where coefficients $S_m(\omega)$ are found as follows. Applying to Eq. (8) the integral operator $\int dV' \Phi_m(\mathbf{r}') \Delta'$, and using the relation

$$\int dV' \Phi_m(\mathbf{r}') \Delta' S_{\text{pl}}(\omega; \mathbf{r}, \mathbf{r}') = -S_m \Phi_m(\mathbf{r}) \int dV \mathbf{E}_m^2(\mathbf{r}) \quad (10)$$

for the left hand side, and the relation

$$\int dV' \Phi_m(\mathbf{r}') \Delta' S_0(\omega; \mathbf{r}, \mathbf{r}') = 4\pi \Phi_m(\mathbf{r}) \quad (11)$$

for the right hand side, we obtain

$$S_m \nabla \cdot [\varepsilon(\omega, \mathbf{r}) \nabla \Phi_m(\mathbf{r})] = 4\pi \frac{\nabla \cdot [(\varepsilon(\omega, \mathbf{r}) - 1) \nabla \Phi_m(\mathbf{r})]}{\int dV \mathbf{E}_m^2(\mathbf{r})}. \quad (12)$$

Finally, multiplying Eq. (12) by $\Phi_m(\mathbf{r})$ and integrating the result over \mathbf{r} , we obtain

$$S_m(\omega) = \frac{4\pi}{\int dV \mathbf{E}_m^2(\mathbf{r})} - \frac{4\pi}{\int dV \varepsilon(\omega, \mathbf{r}) \mathbf{E}_m^2(\mathbf{r})}. \quad (13)$$

For *real* $\varepsilon(\omega, \mathbf{r})$, the Green function (9) with coefficients (13) is *exact* for any metal-dielectric structure with eigenmodes defined by Eq. (6). The first term in Eq. (13) ensures that $S_m = 0$ in the limit $\omega \rightarrow \infty$ (or, in free space with $\varepsilon = 1$), while the second term develops a pole, due to the Gauss law (6), as $|\omega|$ approaches ω_m .

B. Plasmon Green function: including the losses

For complex dielectric function, the plasmon poles in the Green function move into lower half of complex frequency plane. We assume that the mode quality factors Q_m is sufficiently large and so, in the first order in $1/Q_m$, the eigenmodes Φ_m in the Green function expansion (9) are unchanged while the coefficients S_m in Eq. (13) are now complex. Expanding the dielectric function near ω_m ,

$$\varepsilon(\omega, \mathbf{r}) \approx \varepsilon'(\omega_m, \mathbf{r}) + \frac{\partial \varepsilon'(\omega_m, \mathbf{r})}{\partial \omega_m^2} (\omega^2 - \omega_m^2) + i\varepsilon''(\omega, \mathbf{r}), \quad (14)$$

the coefficients (13) take the form

$$S_m(\omega) = \frac{\omega_m^2}{2U_m} \frac{1}{\omega_m^2 - \omega^2 - i\omega\gamma_m^{nr}(\omega)}, \quad (15)$$

where

$$\begin{aligned} U_m &= \frac{\omega_m}{16\pi} \int dV \frac{\partial \varepsilon'(\omega_m, \mathbf{r})}{\partial \omega_m} \mathbf{E}_m^2(\mathbf{r}) \\ &= \frac{1}{16\pi} \int dV \frac{\partial [\omega_m \varepsilon'(\omega_m, \mathbf{r})]}{\partial \omega_m} \mathbf{E}_m^2(\mathbf{r}) \end{aligned} \quad (16)$$

is the plasmon mode energy [51], and the rate

$$\gamma_m^{nr}(\omega) = \frac{2\omega_m \int dV \varepsilon''(\omega, \mathbf{r}) \mathbf{E}_m^2(\mathbf{r})}{\omega \int dV [\partial \varepsilon'(\omega_m, \mathbf{r}) / \partial \omega_m] \mathbf{E}_m^2(\mathbf{r})} \quad (17)$$

describes *nonradiative* plasmon decay at frequency ω . Introducing the power dissipated by the plasmon mode due to nonradiative (Ohmic) losses as [51]

$$W_m^{nr}(\omega) = \frac{\omega}{8\pi} \int dV \varepsilon''(\omega, \mathbf{r}) \mathbf{E}_m^2(\mathbf{r}), \quad (18)$$

the frequency-dependent nonradiative plasmon decay rate (17) can be written in the form

$$\gamma_m^{nr}(\omega) = \frac{\omega_m^2}{\omega^2} \frac{W_m^{nr}(\omega)}{U_m}, \quad (19)$$

which is convenient for extension in the next section.

The quasistatic dyadic Green function for the electric fields is given by $\bar{\mathbf{D}}_{\text{pl}}(\omega; \mathbf{r}, \mathbf{r}') = \nabla \nabla' S_{\text{pl}}(\omega; \mathbf{r}, \mathbf{r}')$, where $S_{\text{pl}}(\omega; \mathbf{r}, \mathbf{r}')$ is given by Eq. (9) with coefficients $S_m(\omega)$ given by Eq. (15), and has the form

$$\bar{\mathbf{D}}_{\text{pl}}(\omega; \mathbf{r}, \mathbf{r}') = \sum_m \frac{\omega_m^2}{2U_m} \frac{\mathbf{E}_m(\mathbf{r}) \mathbf{E}_m(\mathbf{r}')}{\omega_m^2 - \omega^2 - i\omega\gamma_m^{nr}(\omega)}. \quad (20)$$

Note that the coefficients (15) are obtained by calculating the residues at the plasmon poles of function $S_m(\omega)$, given by Eq. (13), and the Green function (20) is obtained by summing up the contributions from all poles. Since the plasmon Green function is analytic in the complex frequency plane except isolated poles in the lower half-plane [for local dielectric function $\varepsilon(\omega, \mathbf{r})$], the expression (20) is valid for *all* frequencies. The functional form of the decay rate (17) along with modes' orthogonality ensures that $\bar{\mathbf{D}}_{\text{pl}}(\omega; \mathbf{r}, \mathbf{r}')$ obeys the optical theorem [52]

$$\begin{aligned} \int dV \varepsilon''(\omega, \mathbf{r}) \bar{\mathbf{D}}_{\text{pl}}^*(\omega; \mathbf{r}, \mathbf{r}') \bar{\mathbf{D}}_{\text{pl}}(\omega; \mathbf{r}, \mathbf{r}'') \\ = 4\pi \text{Im} \bar{\mathbf{D}}_{\text{pl}}(\omega; \mathbf{r}', \mathbf{r}''), \end{aligned} \quad (21)$$

which, in the absence of radiation, implies that system's energy intake (right-hand side) is dissipated via Ohmic losses (left-hand side) [53].

In the following, we assume that QE's interaction with plasmonic system is dominated by a single mode and, accordingly, keep only the resonant term in Eq. (20),

$$\bar{\mathbf{D}}_m(\omega; \mathbf{r}, \mathbf{r}') = \frac{\omega_m^2}{2U_m} \frac{\mathbf{E}_m(\mathbf{r}) \mathbf{E}_m(\mathbf{r}')}{\omega_m^2 - \omega^2 - i\omega\gamma_m(\omega)}, \quad (22)$$

where $\gamma_m(\omega) = \gamma_m^{nr}(\omega)$ for quasistatic case. For well-defined plasmon mode, i.e., if the quality factor is sufficiently large ($\omega_m/\gamma_m \gg 1$), the contribution from negative frequencies is small and the plasmon Green function near the resonance takes the form [50]

$$\bar{\mathbf{D}}_m(\omega; \mathbf{r}, \mathbf{r}') = \frac{\omega_m}{4U_m} \frac{\mathbf{E}_m(\mathbf{r}) \mathbf{E}_m(\mathbf{r}')}{\omega_m - \omega - i\gamma_m/2}, \quad (23)$$

where $\gamma_m = W_m/U_m$ is the plasmon decay rate at plasmon frequency [with $W_m \equiv W_m^{nr}(\omega_m)$ in the quasistatic case]. Note that single-mode Green functions (22) and (23) satisfy the optical theorem (21) as well (the latter with $\omega = \omega_m$). Finally, since only metallic regions with dispersive dielectric function $\varepsilon(\omega) = \varepsilon'(\omega) + i\varepsilon''(\omega)$ contribute to U_m and W_m^{nr} , the standard plasmon decay rate due to nonradiative losses in metal is recovered,

$$\gamma_m^{nr} = \frac{2\varepsilon''(\omega_m)}{\partial\varepsilon'(\omega_m)/\partial\omega_m}. \quad (24)$$

In the next section, we generalize our approach to include plasmon interaction with the radiation field.

III. INTERACTION OF PLASMON MODE WITH RADIATION FIELD

In this section, we demonstrate that the quasistatic Green function (22) can be extended to incorporate the plasmon coupling to radiation field by including plasmon's *radiative* decay rate into full decay rate as follows [compare to Eq. (19)]:

$$\gamma_m(\omega) = \frac{\omega_m^2 W_m(\omega)}{\omega^2 U_m}, \quad (25)$$

where $W_m(\omega) = W_m^{nr}(\omega) + W_m^r(\omega)$ is the *full* dissipated power, which now includes radiated power $W_m^r(\omega)$ that determines plasmon's radiative decay rate as

$$\gamma_m^r(\omega) = \frac{\omega_m^2 W_m^r(\omega)}{\omega^2 U_m}. \quad (26)$$

Below, we derive explicit expressions for radiated power $W_m^r(\omega)$ as well as for optical polarizability of a plasmon mode characterizing plasmonic system's response to an external field.

A. Radiative decay of plasmon mode

We start with noting that emission of light from a plasmonic system with characteristic size much smaller than the radiation wavelength can be treated similarly to a point dipole. The frequency-dependent polarization vector of plasmon mode (6) is $\mathbf{P}_m(\omega, \mathbf{r}) = \chi'(\omega, \mathbf{r})\mathbf{E}_m(\mathbf{r})$, where $\chi(\omega, \mathbf{r}) = [\varepsilon(\omega, \mathbf{r}) - 1]/4\pi$ is plasmonic system's susceptibility that vanishes outside the system (we assume, for simplicity, that dielectric constant of outside medium is unity). Note that, in the plasmon spectral domain $\varepsilon''(\omega)/\varepsilon'(\omega) \ll 1$, the radiation and scattering by a plasmonic dipole are determined, within our approximation, by the real part of susceptibility $\chi' = (\varepsilon' - 1)/4\pi$ whereas its imaginary part $\chi'' = \varepsilon''/4\pi$ determines the Ohmic losses (18). The electric field generated by plasmonic system's oscillating polarization vector is given by

$$\mathbf{E}_m(\omega, \mathbf{r}) = \int dV' \bar{\mathbf{D}}_0(\omega; \mathbf{r}, \mathbf{r}') \cdot \mathbf{P}_m(\omega, \mathbf{r}'), \quad (27)$$

where $\bar{\mathbf{D}}_0(\omega; \mathbf{r}, \mathbf{r}') = (4\pi\omega^2/c^2)\bar{\mathbf{G}}_0(\omega; \mathbf{r}, \mathbf{r}')$ is the free-space dyadic Green function. The power dissipated by the plasmon mode via radiation is given by [37]

$$\begin{aligned} W_m^r(\omega) &= \frac{\omega}{2} \text{Im} \int dV \mathbf{E}_m(\omega, \mathbf{r}) \cdot \mathbf{P}_m(\omega, \mathbf{r}) \\ &= \frac{\omega}{2} \text{Im} \int dV \int dV' \mathbf{P}_m(\omega, \mathbf{r}) \cdot \bar{\mathbf{D}}_0(\omega; \mathbf{r}, \mathbf{r}') \cdot \mathbf{P}_m(\omega, \mathbf{r}'), \end{aligned} \quad (28)$$

where integration takes place over the plasmonic system volume. Replacing the free-space Green function by its near-field limit, $\text{Im}\bar{\mathbf{D}}_0(\omega; \mathbf{r}, \mathbf{r}') = (2\omega^3/3c^3)\mathbf{I}$, we obtain

$$W_m^r(\omega) = \frac{\omega^4}{3c^3} \mathcal{P}_m^2(\omega), \quad (29)$$

where

$$\mathcal{P}_m(\omega) = \int dV \mathbf{P}_m(\omega, \mathbf{r}) = \frac{1}{4\pi} \int dV [\varepsilon'(\omega, \mathbf{r}) - 1] \mathbf{E}_m(\mathbf{r}) \quad (30)$$

is plasmon's dipole moment. Same result is obtained by integrating Poynting's vector $\mathbf{S} = (c/8\pi) |\mathbf{E}_m(\omega, \mathbf{r})|^2$ over remote surface enclosing the system. Note that plasmon's radiated power (29) coincides with that of a point dipole $\mathcal{P}_m(\omega)$, and that, for small systems, radiation of higher-order multipoles is suppressed [37]. By including the radiated power (29) into full dissipated power, the radiative decay channel is incorporated, through the decay rate (25), within the plasmon Green function (22) in a way that ensures energy flux conservation (see below).

Near plasmon resonance, the plasmon decay rate in the Green function (23) takes the form $\gamma_m = \gamma_m^{nr} + \gamma_m^r$, where the plasmon radiation rate is obtained by normalizing the radiated power with the mode energy,

$$\gamma_m^r = \frac{W_m^r}{U_m} = \frac{\omega_m^4 \mathcal{P}_m^2}{3c^3 U_m}, \quad (31)$$

which, upon using Eqs. (16) and (30), takes the form

$$\gamma_m^r = \frac{\omega_m^4}{3\pi c^3} \frac{[\int dV (\varepsilon' - 1) \mathbf{E}_m(\mathbf{r})]^2}{\int dV (\partial\omega_m \varepsilon' / \partial\omega_m) \mathbf{E}_m^2(\mathbf{r})}, \quad (32)$$

where we denoted $W_m^r \equiv W_m^r(\omega_m)$, $\mathcal{P}_m \equiv \mathcal{P}_m(\omega_m)$ and, under the integral, $\varepsilon \equiv \varepsilon(\omega_m, \mathbf{r})$. Correspondingly, the plasmon radiation efficiency η_m has the form

$$\eta_m = \frac{\gamma_m^r}{\gamma_m} = \frac{\zeta_m}{1 + \zeta_m}, \quad (33)$$

where the parameter

$$\zeta_m = \frac{\gamma_m^r}{\gamma_m^{nr}} = \frac{\omega_m^3}{6\pi c^3} \frac{[\int dV (\varepsilon' - 1) \mathbf{E}_m(\mathbf{r})]^2}{\int dV \varepsilon'' \mathbf{E}_m^2(\mathbf{r})}, \quad (34)$$

characterizes plasmon's radiative decay rate vs. nonradiative one. Note that, for small nanoplasmonic systems, γ_m^{nr} should also include the Landau damping rate [54].

As an example, for dipole surface plasmon in a spherical nanoparticle of radius a , a straightforward calculation recovers the radiative decay rate as (see Appendix)

$$\gamma_{sp}^r = \frac{4\omega_{sp}^3 a^3}{c^3 \partial \varepsilon'(\omega_{sp}) / \partial \omega_{sp}}, \quad (35)$$

and, correspondingly, $\zeta_{sp} = 2\omega_{sp}^3 a^3 / c^3 \varepsilon''(\omega_{sp})$, where the plasmon frequency ω_{sp} is given by $\varepsilon'(\omega_{sp}) = -2$.

Finally note that, in contrast to field-independent non-radiative decay rate (24), the radiative decay rate (32) *does* depend on the plasmon field distribution in the system, albeit not on its overall magnitude. Such "nonanalytic" field dependence of γ_m^r , which is present in the Landau damping rate as well [54], reflects the fact that, in contrast to a point dipole, the local fields vary appreciably on the plasmonic system scale.

B. Optical polarizability of a plasmonic system in the external field and energy flux conservation

Here we show that the plasmon Green function that incorporates the Ohmic and radiation losses ensures the standard relation between plasmon's absorption, scattering and extinction cross sections, $\sigma_{abs} + \sigma_{sc} = \sigma_{ext}$, and derive the optical polarizability of plasmon mode which describes plasmonic system's resonant response to an external field. For frequency close to the plasmon resonance, we use the single-mode plasmon Green function (22) and, accordingly, omit non-resonant contributions.

1. Extinction cross section and energy flux conservation

Consider response of a plasmonic system to incident monochromatic field $\mathcal{E}_i e^{-i\omega t}$ that is uniform on the system scale. The electric field scattered by the plasmonic system has the form

$$\mathcal{E}_{sc}(\omega, \mathbf{r}) = \int dV' \chi'(\omega, \mathbf{r}') \bar{\mathbf{D}}(\omega; \mathbf{r}, \mathbf{r}') \cdot \mathcal{E}_i, \quad (36)$$

where $\bar{\mathbf{D}}(\omega; \mathbf{r}, \mathbf{r}')$ is the dyadic Green function (4). The power absorbed by plasmonic structure is

$$P_{abs}(\omega) = \frac{\omega}{8\pi} \int dV \varepsilon''(\omega, \mathbf{r}) |\mathcal{E}_{sc}(\omega, \mathbf{r})|^2, \quad (37)$$

where we disregarded nonresonant direct field absorption. Inside the plasmonic system, for each mode, we replace $\bar{\mathbf{D}}(\omega; \mathbf{r}, \mathbf{r}')$ in Eq. (36) with the plasmon Green function $\bar{\mathbf{D}}_m(\omega; \mathbf{r}, \mathbf{r}')$, given by Eq. (22), and obtain

$$P_{abs}(\omega) = W_m^{nr}(\omega) |S_m(\omega)|^2 [\mathcal{P}_m(\omega) \cdot \mathcal{E}_i]^2, \quad (38)$$

where the functions $S_m(\omega)$, $W_m^{nr}(\omega)$, and $\mathcal{P}_m(\omega)$ are given by Eqs. (15), (18) and (30), respectively. Normalizing $P_{abs}(\omega)$ by incident energy flux $S_i = (c/8\pi) \mathcal{E}_i^2$, we

obtain the mode *absorption* cross section

$$\sigma_{abs}^{(m)}(\omega) = \frac{4\pi\omega}{c} \frac{\omega_m^2}{2U_m} \frac{\omega \gamma_m^{nr}(\omega) [\mathbf{e} \cdot \mathcal{P}_m(\omega)]^2}{(\omega_m^2 - \omega^2)^2 + \omega^2 \gamma_m^2(\omega)}, \quad (39)$$

where plasmon decay rates $\gamma_m^{nr}(\omega)$ and $\gamma_m(\omega)$ are given by Eqs. (19) and (25), respectively, and unit vector \mathbf{e} is the incident field polarization.

To obtain scattering cross section, we extract the far field contribution from Eq. (36) with help of the Dyson equation for dyadic Green function,

$$\begin{aligned} \bar{\mathbf{D}}(\omega; \mathbf{r}, \mathbf{r}') &= \bar{\mathbf{D}}_0(\omega; \mathbf{r}, \mathbf{r}') \\ &+ \int dV_1 \chi'(\omega, \mathbf{r}_1) \bar{\mathbf{D}}_0(\omega; \mathbf{r}, \mathbf{r}_1) \cdot \bar{\mathbf{D}}(\omega; \mathbf{r}_1, \mathbf{r}'). \end{aligned} \quad (40)$$

Keeping only the resonance (second) term and replacing $\bar{\mathbf{D}}(\omega; \mathbf{r}_1, \mathbf{r}')$ with the plasmon Green function (22), we integrate the energy flux $S = (c/8\pi) |\mathcal{E}_{sc}(\omega, \mathbf{r})|^2$ over remote surface enclosing the system. Using far field asymptotics $\bar{\mathbf{D}}_0(\omega; \mathbf{r}) \sim (\omega/c)^2 (e^{ikr}/r) (\mathbf{I} - \hat{\mathbf{r}}\hat{\mathbf{r}})$, we obtain

$$P_{sc}(\omega) = W_m^r(\omega) |S_m(\omega)|^2 [\mathcal{P}_m(\omega) \cdot \mathcal{E}_i]^2, \quad (41)$$

where $W_m^r(\omega)$ is given by Eq. (29). Normalizing $P_{sc}(\omega)$ by S_i , we obtain the mode *scattering* cross section

$$\sigma_{sc}^{(m)}(\omega) = \frac{4\pi\omega}{c} \frac{\omega_m^2}{2U_m} \frac{\omega \gamma_m^r(\omega) [\mathbf{e} \cdot \mathcal{P}_m(\omega)]^2}{(\omega_m^2 - \omega^2)^2 + \omega^2 \gamma_m^2(\omega)}, \quad (42)$$

where the plasmon radiative decay rate $\gamma_m^r(\omega)$ is given by Eq. (26). Adding $\sigma_{sc}^{(m)}(\omega)$ and $\sigma_{abs}^{(m)}(\omega)$ together, we obtain the mode *extinction* cross section as

$$\sigma_{ext}^{(m)}(\omega) = \frac{4\pi\omega}{c} \frac{\omega_m^2}{2U_m} \frac{\omega \gamma_m(\omega) [\mathbf{e} \cdot \mathcal{P}_m(\omega)]^2}{(\omega_m^2 - \omega^2)^2 + \omega^2 \gamma_m^2(\omega)}, \quad (43)$$

where we used the relation $\gamma_m(\omega) = \gamma_m^{nr}(\omega) + \gamma_m^r(\omega)$, which, in this case, implies the energy flux conservation:

$$\sigma_{abs}^{(m)}(\omega) = \frac{\gamma_m^{nr}(\omega)}{\gamma_m(\omega)} \sigma_{ext}^{(m)}(\omega), \quad \sigma_{sc}^{(m)}(\omega) = \frac{\gamma_m^r(\omega)}{\gamma_m(\omega)} \sigma_{ext}^{(m)}(\omega). \quad (44)$$

The full cross sections σ_{abs} , σ_{sc} and σ_{ext} are obtained by summing up Eqs. (39), (42) and (43) over all modes.

2. Optical polarizability of plasmonic system

We can now obtain optical response functions of plasmonic system by using the standard relation

$$\sigma_{ext}(\omega) = \frac{4\pi\omega}{c} \text{Im}[\mathbf{e} \cdot \bar{\boldsymbol{\alpha}}(\omega) \cdot \mathbf{e}], \quad (45)$$

where $\bar{\boldsymbol{\alpha}}(\omega) = \sum_m \bar{\boldsymbol{\alpha}}_m(\omega)$ is optical polarizability dyadic, which characterizes plasmonic system's response to an external field. From Eq. (43), the plasmon mode polarizability is obtained explicitly as

$$\bar{\boldsymbol{\alpha}}_m(\omega) = \frac{\omega_m^2}{2U_m} \frac{\mathcal{P}_m(\omega) \mathcal{P}_m(\omega)}{\omega_m^2 - \omega^2 - i\omega \gamma_m(\omega)}. \quad (46)$$

The mode polarizability (46) can be split into scattering and absorbing parts as (suppressing ω -dependence)

$$\bar{\alpha}_m'' = \frac{\gamma_m^r}{\gamma_m} \bar{\alpha}_m'' + \frac{\gamma_m^{nr}}{\gamma_m} \bar{\alpha}_m'', \quad (47)$$

where the first term represents the scattering contribution and satisfies the relation

$$\frac{\gamma_m^r}{\gamma_m} \bar{\alpha}_m'' = \frac{2}{3} \left(\frac{\omega}{c}\right)^3 \bar{\alpha}_m \cdot \bar{\alpha}_m^*. \quad (48)$$

Since $\bar{\alpha}_m$ is proportional to plasmonic system's volume, the scattering is suppressed for small systems. In this case, the extinction is dominated by the absorption, which is given by the second term in Eq. (47). Near the resonance, the mode polarizability takes the form

$$\bar{\alpha}_m(\omega) = \frac{\omega_m}{4U_m} \frac{\mathcal{P}_m \mathcal{P}_m}{\omega_m - \omega - i\gamma_m/2}, \quad (49)$$

and, after summing up over all modes, can be used to characterize linear response of any plasmonic system supporting well-defined plasmon modes.

Radiative decay contribution into full polarizability, $\alpha(\omega) = \text{Tr}[\bar{\alpha}(\omega)]$, can be expressed in general form in terms of quasistatic polarizabilities $\tilde{\alpha}_m(\omega)$. Taking the trace of Eq. (46), $\alpha(\omega)$ can be written as

$$\alpha_m(\omega) = \frac{\tilde{\alpha}_m(\omega)}{1 - i\frac{2\omega^3}{3c^3} \tilde{\alpha}_m(\omega)}, \quad (50)$$

where

$$\tilde{\alpha}_m(\omega) = \frac{\omega_m^2}{2U_m} \frac{\mathcal{P}_m^2(\omega)}{\omega_m^2 - \omega^2 - i\omega\gamma_m^{nr}(\omega)} \quad (51)$$

is plasmon polarizability *without* radiative decay. The relation (50) is similar to that for dipole polarizability of spherical particles [27] but, in fact, it holds for any nanoplasmonic system. In a similar manner, $\alpha_m(\omega)$ can be shown to satisfy the optical theorem

$$\alpha_m''(\omega) = \frac{2}{3} \left(\frac{\omega}{c}\right)^3 |\alpha_m(\omega)|^2 + \frac{\tilde{\alpha}_m''(\omega)}{|1 - i\frac{2\omega^3}{3c^3} \tilde{\alpha}_m(\omega)|^2}, \quad (52)$$

where first and second terms in the right hand side describe, respectively, scattering and absorption.

For a nanosphere with $\tilde{\alpha}_m(\omega) = a^3[\varepsilon(\omega) - 1]/[\varepsilon(\omega) + 2]$, by expanding $\varepsilon(\omega)$ near ω_{sp} , we obtain from Eq. (50)

$$\alpha_{sp}(\omega) = \frac{3a^3}{\partial\varepsilon'(\omega_{sp})/\partial\omega_{sp}} \frac{1}{\omega_{sp} - \omega - i\gamma_{sp}/2}, \quad (53)$$

where $\gamma_{sp} = \gamma_{sp}^{nr} + \gamma_{sp}^r$ is the plasmon full decay rate with nonradiative and radiative contributions given by Eqs. (24) and (35), respectively. Same result is obtained directly from Eq. (49) (see Appendix).

The approach developed in this section will be used in the rest of this paper to describe spontaneous decay of a QE coupled to plasmonic resonator.

IV. PLASMON LDOS, MODE DENSITY AND MODE VOLUME

We are now in position to derive the plasmon LDOS that accounts for both Ohmic and radiative losses. On length scale below the diffraction limit, surface plasmons are mostly electronic excitations interacting weakly with the radiation field. In this section we show that, within our approach, the plasmon mode volume can be defined in natural way as the inverse of plasmon mode density, which describes plasmon mode confinement in local region. We derive explicit expression for the plasmon mode volume at a hot spot near sharp metal tip and show that it scales with the metal volume while being highly sensitive to the distance to the tip.

A. Mode volume for plasmonic systems

The standard expression for electromagnetic LDOS, $\rho(\omega, \mathbf{r}) = (2\omega/\pi c^2) \text{ImTr}[\bar{\mathbf{G}}(\omega; \mathbf{r}, \mathbf{r})]$, can be written in terms of rescaled Green dyadic (4) as

$$\rho(\omega, \mathbf{r}) = \frac{1}{2\pi^2\omega} \text{Im Tr } \bar{\mathbf{D}}(\omega; \mathbf{r}, \mathbf{r}). \quad (54)$$

Near plasmon resonance, using the plasmon Green dyadic (23), we obtain the plasmon LDOS as

$$\rho_m(\omega, \mathbf{r}) = \frac{1}{4\pi^2 W_m} \frac{\mathbf{E}_m^2(\mathbf{r})}{1 + 4Q_m^2(\omega/\omega_m - 1)^2}, \quad (55)$$

where the plasmon quality factor is given by

$$Q_m = \frac{\omega_m}{\gamma_m} = \frac{\omega_m U_m}{W_m}, \quad (56)$$

and dissipated power $W_m = W_m^{nr} + W_m^r$ incorporates all plasmon damping channels. As function of frequency, the LDOS has Lorentzian shape and, at resonance, is proportional to the plasmon field intensity normalized by the dissipated power [50]: $\rho(\omega_m, \mathbf{r}) = \mathbf{E}_m^2(\mathbf{r})/4\pi^2 W_m$.

The plasmon LDOS (55) describes plasmon states' distribution in unit volume and frequency interval. Frequency integration of LDOS yields *plasmon mode density*

$$\rho_m(\mathbf{r}) = \int d\omega \rho_m(\omega, \mathbf{r}) = \frac{\omega_m \mathbf{E}_m^2(\mathbf{r})}{8\pi Q_m W_m} = \frac{\mathbf{E}_m^2(\mathbf{r})}{8\pi U_m}, \quad (57)$$

which describes spatial distribution of plasmon field intensity. Note that, in contrast to LDOS, $\rho(\mathbf{r})$ is normalized by the mode energy, rather than dissipated power, and, hence, is *independent of losses*. With help of Eq. (16), the mode density is explicitly obtained as

$$\rho_m(\mathbf{r}) = \frac{1}{\mathcal{V}_m(\mathbf{r})} = \frac{2\mathbf{E}_m^2(\mathbf{r})}{\int dV \mathbf{E}_m^2(\mathbf{r}) \partial(\omega_m \varepsilon')/\partial\omega_m}, \quad (58)$$

and can be viewed as the inverse *local mode volume* $\mathcal{V}_m(\mathbf{r})$, which characterizes field confinement at point \mathbf{r} .

The expression (58) is valid for any nanoplasmonic system, including plasmonic cavities and open systems.

Note that the form (58) for plasmon mode volume was proposed previously in the case of spherical metal nanoshell [42]. For more general systems described by dispersive dielectric function, a similar expression was obtained by using expansion of full Maxwell equations' solution over quasinormal modes (QNM) [29]. Since QNMs are leaky modes described by complex-valued fields, the QNM volume is complex as well, and so the QNM Purcell factor is given by the real part of Eq. (1) [29, 49].

Within our approach, the local mode volume at point \mathbf{r} arises as the inverse of plasmon mode density at that point and, hence, represents *real* function of plasmon field intensity and is independent of radiative and nonradiative losses. These losses still do affect the Purcell factor (1) as they determine the quality factor Q_m via the full plasmon decay rate $\gamma_m = \gamma_m^r + \gamma_m^{nr}$, thereby ensuring the energy flux conservation.

B. Plasmon mode volume near metallic tip

The largest plasmonic enhancements occur if QE is located at a *hot spot* – a small region characterized by very high mode density (or very small mode volume), e.g., near sharp tip of a metal nanostructure. With help of Eq. (58), the maximal mode density can be estimated by assuming classical field profile near the metal surface. Due to the Gauss law, the local fields do not significantly change inside small metallic structure, while falling off rapidly outside it, so the highest field intensity is achieved near the metal surface,

$$\rho_m(\mathbf{r}) \approx \frac{2}{\omega_m \partial \varepsilon'(\omega_m) / \partial \omega_m} \frac{E_L^2(\mathbf{r}) + E_T^2(\mathbf{r})}{V_{\text{met}} ([E_L^{\text{in}}]^2 + E_T^2)}, \quad (59)$$

where V_{met} is the metal volume. Here, subscripts L and T stand for longitudinal (normal to the tip) and transverse (tangential to the tip) field components, and superscripts *in* and *out* indicate local fields at the interface on metal and dielectric side, respectively. The highest field localization is achieved when E_T , which is continuous across the metal-dielectric interface, is much smaller than E_L . Assuming that the local field is polarized along the tip, i.e., $E_L \gg E_T$, and using boundary condition for normal field component $E_L^{\text{out}} = \varepsilon'(\omega_m) E_L^{\text{in}}$, we obtain the mode density projected along the tip:

$$\rho_L(\mathbf{r}) = \frac{1}{\mathcal{V}_L(\mathbf{r})} = \frac{1}{V_{\text{met}}} \frac{2|\varepsilon'(\omega_m)|^2 \tilde{E}_L^2(\mathbf{r})}{\omega_m \partial \varepsilon'(\omega_m) / \partial \omega_m}, \quad (60)$$

where $\tilde{E}_L(\mathbf{r}) = E_L(\mathbf{r})/E_L^{\text{out}}$ is normal field component at point \mathbf{r} near the tip normalized by its value at the tip. Although the mode volume near hot spot scales with the metal volume V_{met} , the ratio $V_{\text{met}}/\mathcal{V}_L = V_{\text{met}}\rho_L$ depends on the proximity of QE to the tip. While the mode density is highest at the tip ($\tilde{E}_L = 1$), it is expected to saturate below distances $\sim v_F/\omega$ as the nonlocal effects

become dominant [55, 56]. Note for noble metals, this length scale is ~ 1 nm in the plasmonic frequency range.

V. PURCELL FACTOR AND ENHANCEMENT FACTOR FOR POWER SPECTRUM

Purcell factor characterizes the enhancement of QE decay rate due to ET between QE and plasmonic resonator. Part of transferred energy is radiated away by the plasmonic antenna, while the rest is dissipated due to the Ohmic losses in metal. In this section, we derive explicit expressions for Purcell factor for spontaneous decay rate and enhancement factor for radiated power spectrum. In this paper, we only consider weak coupling regime and disregard plasmon back action on QE spectrum.

A. QE-plasmon ET rate and Purcell factor

The ET rate between a QE situated at \mathbf{r}_0 with dipole moment $\mathbf{p} = \mu \mathbf{n}$ and resonant plasmon mode is straightforwardly obtained from Eq. (5) using the plasmon Green function (23) as

$$\gamma_{et}(\omega) = \frac{\mu^2 Q_m}{\hbar U_m} \frac{[\mathbf{n} \cdot \mathbf{E}_m(\mathbf{r}_0)]^2}{1 + 4Q_m^2(\omega/\omega_m - 1)^2}. \quad (61)$$

As function of QE emission frequency ω , the rate (61) has Lorentzian shape with maximum at $\omega = \omega_m$. In terms of mode volume projected on QE dipole direction \mathbf{n} ,

$$\rho_m^n(\mathbf{r}) = \frac{1}{\mathcal{V}_m^n(\mathbf{r})} = \frac{2[\mathbf{n} \cdot \mathbf{E}_m(\mathbf{r})]^2}{\int dV \mathbf{E}_m^2 \partial(\omega_m \varepsilon') / \partial \omega_m}, \quad (62)$$

the QE-plasmon ET rate takes the form

$$\gamma_{et}(\omega) = \frac{8\pi\mu^2}{\hbar \mathcal{V}_m^n(\mathbf{r}_0)} \frac{Q_m}{1 + 4Q_m^2(\omega/\omega_m - 1)^2}. \quad (63)$$

Normalizing the QE-plasmon ET rate at resonance frequency, $\gamma_{et}(\omega_m) = 8\pi\mu^2 Q_m / \hbar \mathcal{V}_m^n$, by the free-space QE spontaneous decay rate (3), we finally obtain the Purcell factor for a QE coupled to resonant plasmon mode,

$$F_p = \frac{6\pi Q_m}{k^3 \mathcal{V}_m^n} = \frac{12\pi Q_m [\mathbf{n} \cdot \mathbf{E}_m(\mathbf{r}_0)]^2}{k^3 \int dV \mathbf{E}_m^2 \partial(\omega_m \varepsilon') / \partial \omega_m}, \quad (64)$$

which extends the cavity Purcell factor (1) to plasmonic resonators. For QE at the hot spot near metallic tip, with help of Eq. (60), we obtain

$$F_p^{\text{tip}} = \frac{12\pi Q_m |\varepsilon'(\omega_m)|^2}{k^3 V_{\text{met}} \omega_m \partial \varepsilon'(\omega_m) / \partial \omega_m} [\mathbf{n} \cdot \tilde{\mathbf{E}}_L(\mathbf{r}_0)]^2, \quad (65)$$

where $\mathbf{n} \cdot \tilde{\mathbf{E}}_L(\mathbf{r}_0)$ stands for projection of normalized field component along the tip onto QE's dipole orientation \mathbf{n} . The Purcell factor is maximal when QE dipole is oriented along the tip while, for transverse dipole orientation, there is no significant enhancement.

B. Radiated power spectrum

Part of the energy transferred from QE to resonant plasmon mode is radiated away by the plasmonic antenna, leading to overall enhancement of radiated power observed, e.g., in plasmon-enhanced fluorescence experiments [5–11]. While plasmon's radiative decay rate (31) is typically much larger than that of individual QE, i.e., $\gamma_m^r \gg \gamma_0^r$, significant part of the transferred energy is dissipated in the metal at rate (24), so that the enhancement factor depends on radiation efficiency of the plasmonic antenna $\eta_m = \gamma_m^r/\gamma_m$.

The power radiated by a QE placed at position \mathbf{r}_0 near plasmonic antenna is obtained by integrating Poynting's vector $S = (c/8\pi)|\mathcal{E}(\mathbf{r})|^2$ over remote surface enclosing the system, where $\mathcal{E}(\mathbf{r})$ is the QE electric field [37]

$$\mathcal{E}(\mathbf{r}) = \bar{\mathbf{D}}(\omega; \mathbf{r}, \mathbf{r}_0) \cdot \mathbf{p}, \quad (66)$$

and $\bar{\mathbf{D}}(\omega; \mathbf{r}, \mathbf{r}_0)$ is the Green dyadic (4). In order to extract far field contribution, we use the Dyson equation (40). Replacing the near-field Green dyadic $\bar{\mathbf{D}}$ in the integrand by plasmon Green dyadic (23), the QE-generated far field (66) takes the form

$$\begin{aligned} \mathcal{E}(\mathbf{r}) = & \bar{\mathbf{D}}_0(\omega; \mathbf{r} - \mathbf{r}_0) \cdot \mathbf{p} \\ & + \frac{\omega_m}{4U_m} \frac{\mathbf{E}_m(\mathbf{r}_0) \cdot \mathbf{p}}{\omega_m - \omega - i\gamma_m/2} \int dV' \bar{\mathbf{D}}_0(\omega; \mathbf{r} - \mathbf{r}') \cdot \mathbf{P}_m(\mathbf{r}'). \end{aligned} \quad (67)$$

Straightforward integration of Poynting's vector over remote spherical surface yields the radiated power

$$W_r(\omega) = \frac{\omega^4}{3c^3} \left| \mathbf{p} + \frac{\omega_m}{4U_m} \frac{\mathbf{P}_m[\mathbf{E}_m(\mathbf{r}_0) \cdot \mathbf{p}]}{\omega_m - \omega - i\gamma_m/2} \right|^2, \quad (68)$$

where the second term represents contribution of the plasmonic antenna with dipole moment \mathbf{P}_m . Near the resonance, the plasmon emission is dominant and, disregarding the first nonresonant term, we obtain

$$W_r(\omega) = \frac{\mu^2 \omega^4}{3c^3} \frac{\gamma_m^r \gamma_{et}(\omega)}{\gamma_m \gamma_0^r}, \quad (69)$$

where QE-plasmon ET rate $\gamma_{et}(\omega)$ is given by Eq. (63), and radiative decay rates γ_0^r and γ_m^r are given by Eqs. (3) and (31), respectively. Normalizing $W_r(\omega)$ by spectral power $W_r^0 = \mu^2 \omega^4 / 3c^3$ radiated by an isolated QE [37], we obtain the enhancement factor for power spectrum

$$M(\omega) = \frac{F_p \eta_m}{1 + 4Q_m^2 (\omega/\omega_m - 1)^2}, \quad (70)$$

where the Purcell factor F_p is given by Eq. (64) and plasmon radiation efficiency η_m is given by (33). At the resonance, $|\omega - \omega_m| \ll \gamma_m$, we obtain

$$M(\omega_m) = F_p \eta_m = \frac{6\pi Q_m}{k^3 \mathcal{V}_m^n} \eta_m, \quad (71)$$

which represents general relation between the Purcell factor for spontaneous decay and maximal enhancement factor. For high radiation efficiency $\eta \sim 1$, the enhancement factor is comparable to the Purcell factor, i.e., energy is radiated by the plasmonic antenna at approximately same rate as it is being received from the QE.

Note finally that the relation (71) overestimates the enhancement factor as it does not account for ET from QE to off-resonant modes which leads to radiation quenching at close QE-metal distances. The fraction of energy transferred to bright plasmon mode is $q = F_p / \sum_l F_p^{(l)}$, where $F_p^{(l)}$ are Purcell factors for all modes and so, close to the metal surface, the enhancement factor M is suppressed by the quenching factor q .

VI. NUMERICAL RESULTS AND DISCUSSION

To illustrate our theory, we performed numerical calculations for a QE coupled to longitudinal plasmon mode oscillating, with frequency ω_L , along Au nanorod, which is modeled here by prolate spheroid with semi-major and semi-minor axes a and b , respectively (see schematics in Fig. 1). This needle-shaped structure is characterized by relatively high radiation efficiency while, at the same time, possesses hot spots near the tips, where the plasmon field is highly localized. We assume that Au nanorod is submerged into water ($\varepsilon_s = 1.77$) and use experimental Au dielectric function $\varepsilon(\omega) = \varepsilon'(\omega) + i\varepsilon''(\omega)$ in all calculations. The dielectric constant ε_s of surrounding medium is restored in all expressions via replacements: $c \rightarrow c/\varepsilon_s$, $\varepsilon(\omega, \mathbf{r}) \rightarrow \varepsilon(\omega, \mathbf{r})/\varepsilon_s$, and $\mu^2 \rightarrow \mu^2/\varepsilon_s$. Analytical expressions for spheroidal particles are provided in the Appendix along with other technical detail, and here we only discuss the results of numerical calculations.

In Fig. 1, we show calculated plasmon radiation efficiency $\eta_L = \gamma_L^r/\gamma_L$ and quality factor $Q_L = \omega_L/\gamma_L$ which include both radiative and Ohmic losses. As expected, the increase of η_L [see Fig. 1(a)] due to increase of γ_L^r with nanorod overall size is accompanied by the reduction of quality factor [see Fig. 1(b)] due to overall increase of the plasmon decay rate $\gamma_L = \gamma_L^r + \gamma_L^{nr}$. The maximal values of η_L and Q_L are reached for aspect ratio a/b in the range $3 \div 5$, corresponding to plasmon wavelength range $650 \div 800$ nm. In this range, $\varepsilon''(\omega)$ for Au reaches its minimum, which translates to lowest Ohmic losses and, hence, highest η_L and Q_L , except for the largest nanorod ($a = 50$ nm), where the plasmon decay is dominated by radiative channel [see Fig. 1(b)].

To study the field confinement at hot spot, we plot in Fig. 2 the projected plasmon mode density ρ_L , normalized by the metal volume, as function of distance d to the nanorod tip for several values of aspect ratio. Note that for spheroidal particles, Eq. (60) is exact. To account for field enhancement saturation due to nonlocal effects [55, 56], we restrict minimal distance to the tip by $d_{\min} = 0.05a$, and change the nanorod volume by reducing b at fixed a . For aspect ratios a/b in the range $2 \div 4$,

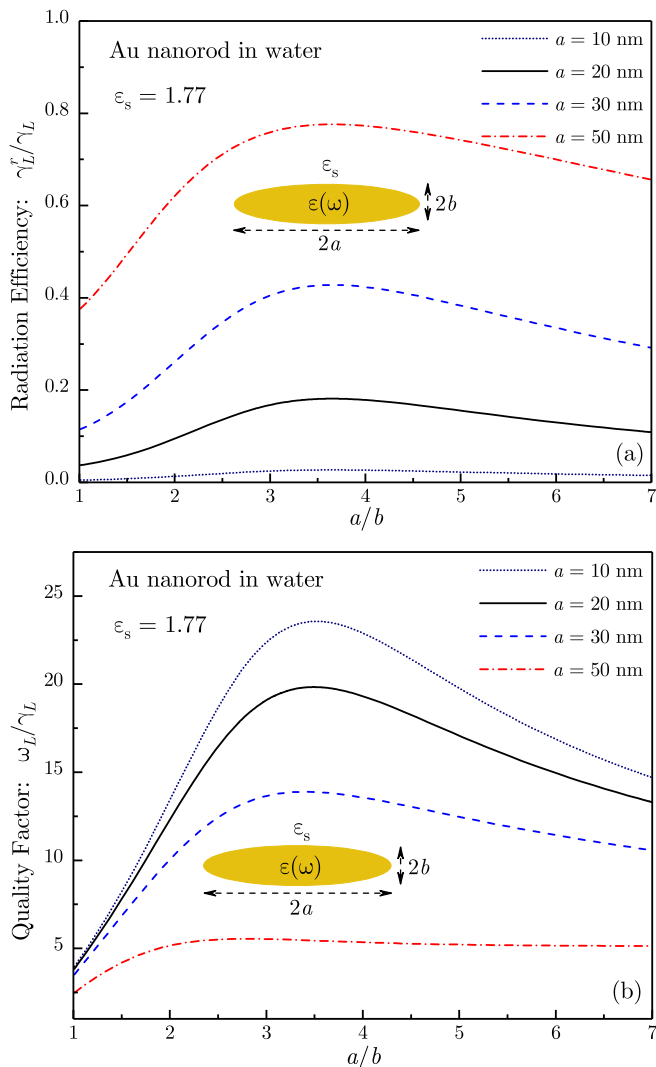


FIG. 1. Plasmon radiation efficiency η_L (a), and quality factor Q_L (b) plotted against aspect ratio a/b for different nanorod sizes. Inset: Schematics of prolate spheroidal particle.

i.e., when hot spots at the tips are well developed, the mode volume $\mathcal{V}_L = 1/\rho_L$ exhibits nearly universal behavior reaching V_{met} in the hot spot region while rapidly decreasing when moving away from the tip.

Consider now spontaneous decay of a QE at distance d from the nanorod tip with its dipole oriented normally to the metal surface (see schematics in Fig. 3). We assume that the QE is situated at fixed distance $d = 1$ nm from the tip, where the plasmon field is highly localized. In Fig. 3, we show the QE-plasmon ET rate (63), normalized by free-space decay rate (3), and the enhancement factor for power spectrum (70) plotted against QE emission frequency ω for different overall sizes but at fixed aspect ratio $a/b = 3.0$. The amplitude of frequency Lorentzian $\gamma_{et}(\omega)/\gamma_0^r$ in Fig. 3(a) is given by the Purcell factor (64), which, near hot spot, scales as Q_L/k^3V_{met} [see Eq. (65)]. With increasing nanorod size, the Purcell factor sharply decreases due to combined effect of decreasing Q_L and, more importantly, increasing k^3V_{met} . However, the en-

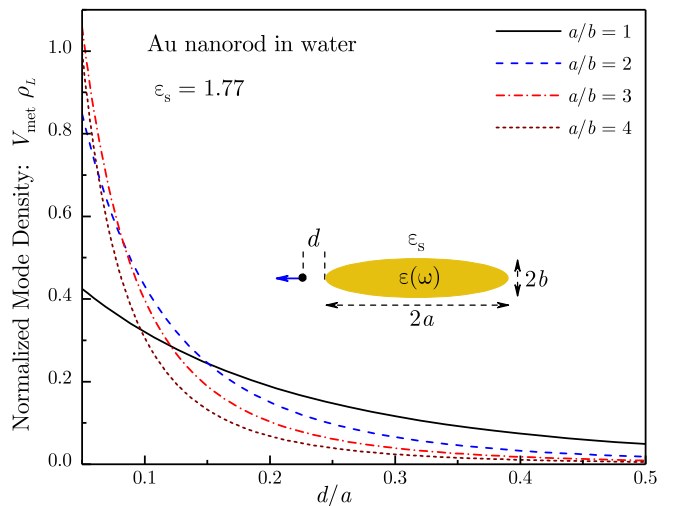


FIG. 2. Normalized mode density (inverse mode volume) projected along Au nanorod is plotted against the distance to nanorod tip for different aspect ratios a/b at fixed a .

hancement factor $M(\omega)$ in Fig. 3(b) exhibits more complicated behavior: its amplitude $F_p\eta_L$ first sharply increases due to rapid change of η_L as a changes from 10 nm to 20 nm, but then, for larger a , falls down as the metal volume effect in F_p takes over.

In Fig. 4, we show the Purcell factor F_p and enhancement factor at resonance frequency $M(\omega_L) = F_p\eta_L$ plotted against the distance d to the nanorod tip for several overall sizes. With QE moving away from the tip, both F_p and $M(\omega_L)$ decrease by up to two orders of magnitude as d increases to $a/2$, indicating that the plasmon field is highly localized near the tips (see Fig. 2). Note that since the distance in Fig. 4 is measured in units of nanorod size, the same starting point $d = 0.05a$ for each curve translates into different initial distance to the metal surface. After appropriate rescaling to bring initial distances to the same numerical value (e.g., 1.0 nm), the order of curves in Fig. 4 follows that in Fig. 3. Overall, Figs. 3 and 4 indicate that the Purcell factor and enhancement factor are highly sensitive to the system size due to scaling of the plasmon mode volume with the metal volume (see Fig. 2) and, to lesser degree, size-dependence of plasmon quality factor and radiation efficiency (see Fig. 1).

VII. CONCLUSIONS

In summary, here we presented a theory for spontaneous decay of a quantum emitter coupled to localized plasmon mode in metal-dielectric structure characterized by dispersive dielectric function which incorporates, in a consistent way, plasmon coupling to the radiation field. For plasmonic systems with characteristic size below the diffraction limit, we derived explicit expressions for plasmon radiative decay rate, which determines radiation efficiency of a plasmonic antenna, and optical polarisability, which defines system response to an external field.

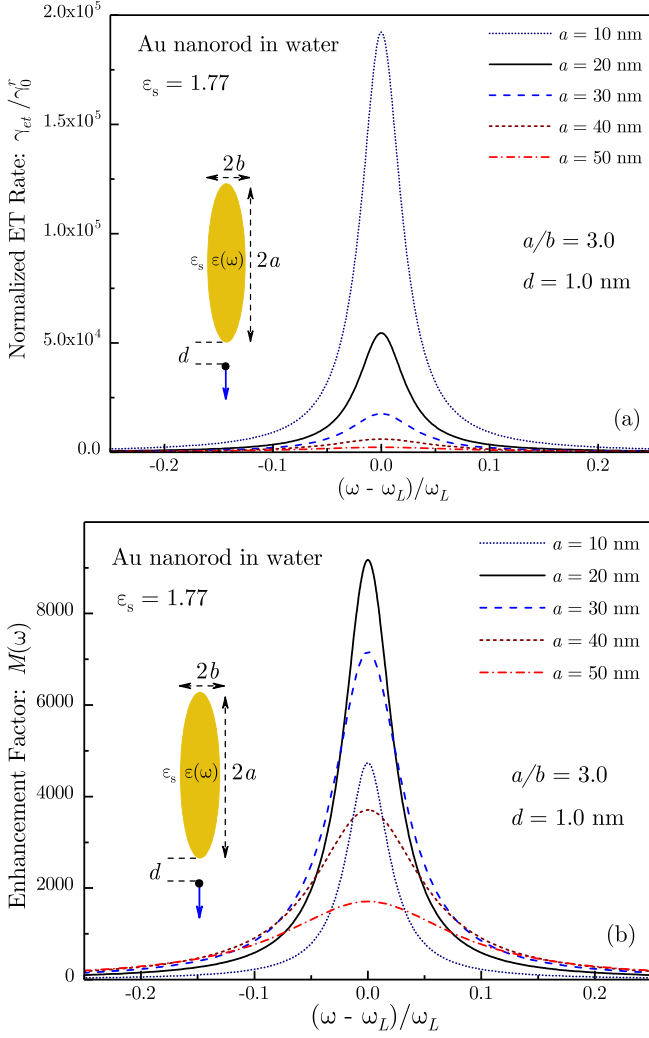


FIG. 3. Frequency dependence of normalized QE-plasmon ET rate and enhancement factor for power spectrum for normally-oriented QE at distance 1.0 nm from Au nanorod tip is plotted for different nanorod sizes and fixed aspect ratio $a/b = 3.0$.

Using these results, we extended our approach [50] to derive plasmon Green function that now includes plasmon interaction with radiation field and obtained explicit expression for the plasmon local density of states that accounts for all relevant plasmon damping channels. We have shown that plasmon mode volume is defined naturally as the inverse of plasmon mode density, which characterized plasmon field confinement, and that, for well-defined plasmon modes, it is independent of losses. We estimated the plasmon mode volume at hot spot near sharp tip of a small metal nanostructure and demonstrated that it scales with the metal volume, although its actual value is highly sensitive to the QE distance to the tip. Using our approach, we recovered the usual form of Purcell factor, but now for plasmonic resonators, and established its relation with the enhancement factor for radiated power. Finally, we illustrated our approach by presenting numerical results for QE situated near the tip of an Au nanorod.

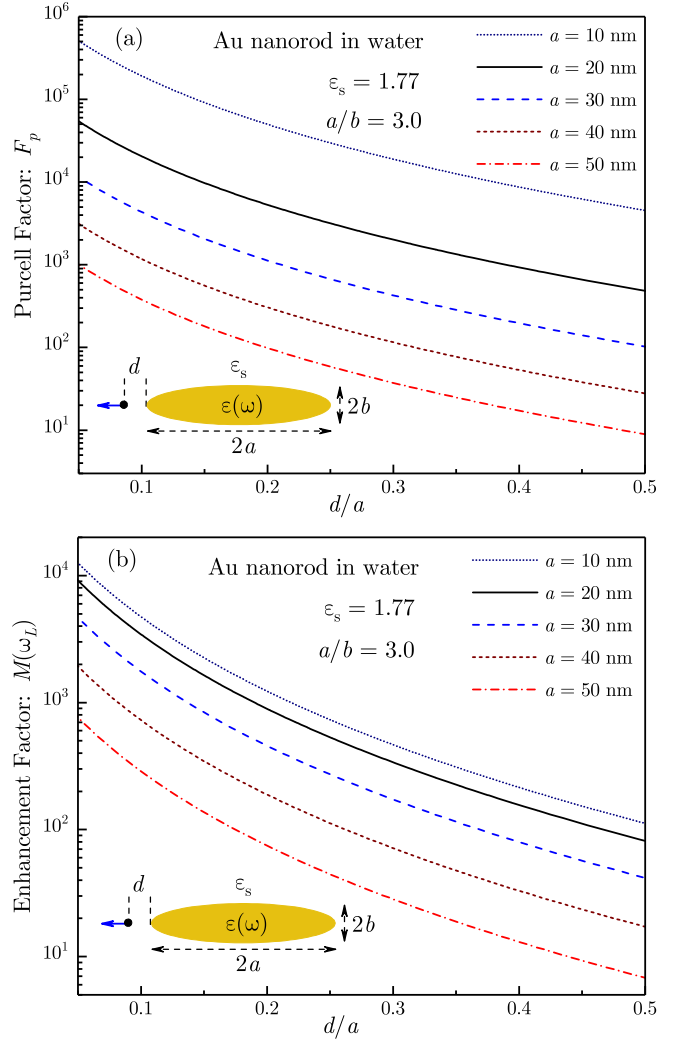


FIG. 4. Distance dependence of Purcell factor and enhancement factor for power spectrum at resonance frequency is plotted for normally-oriented QE at different Au nanorod sizes and fixed aspect ratio a/b .

This work was supported in part by NSF grants No. DMR-1610427 and No. HRD-1547754.

Appendix A: Potentials and fields in nanospheroids

Consider a prolate spheroid with semiaxis a along the symmetry axis and semiaxis b in the symmetry plane ($a > b$). We use standard notations for spheroidal coordinates (ξ, η, ϕ) where ξ is "radial" coordinate while $\eta = \cos \theta$ and ϕ parametrise the surface. The scaling factors are given by

$$\begin{aligned} h_\xi &= f \sqrt{\frac{\xi^2 - \eta^2}{\xi^2 - 1}}, & h_\eta &= f \sqrt{\frac{\xi^2 - \eta^2}{1 - \eta^2}}, \\ h_\phi &= f \sqrt{(\xi^2 - 1)(1 - \eta^2)}, \end{aligned} \quad (\text{A1})$$

where $f = \sqrt{a^2 - b^2}$ is half distance between the foci, and spheroid surface corresponds to $\xi_1 = a/f$. The volume and surface elements are, respectively, $dV = h_\xi h_\eta h_\phi d\xi d\eta d\phi$ and $dS = h_\eta h_\phi d\eta d\phi$, and the gradient operator is $\nabla = \hat{\xi} h_\xi^{-1} \partial/\partial\xi + \hat{\eta} h_\eta^{-1} \partial/\partial\eta + \hat{\phi} h_\phi^{-1} \partial/\partial\phi$.

The potentials for longitudinal and transverse dipole modes are

$$\Phi_L = f R_L(\xi) P_1(\eta), \quad \Phi_T = f R_T(\xi) P_1^1(\eta) \cos\phi. \quad (\text{A2})$$

For a metallic spheroid with permittivity $\varepsilon(\omega)$ in a medium with dielectric constant ε_s , the radial components for longitudinal mode are

$$\begin{aligned} R_L(\xi) &= P_1(\xi), \quad \text{for } \xi < \xi_1, \\ R_L(\xi) &= Q_1(\xi) P_1(\xi_1)/Q_1(\xi_1), \quad \text{for } \xi > \xi_1. \end{aligned} \quad (\text{A3})$$

The plasmon frequencies ω_L follow from the continuity of $\varepsilon R'(\xi)$ across the metal/dielectric interface.

Appendix B: Plasmon energy in spheroidal particles

In the quasistatic approximation, the plasmon mode energy comes solely from the metal and has the form

$$\begin{aligned} U_m &= \frac{\omega_m}{16\pi} \frac{\partial\varepsilon(\omega_m)}{\partial\omega_m} \int dV_{\text{met}} \mathbf{E}_m^2 \\ &= \frac{\omega_m}{16\pi} \frac{\partial\varepsilon(\omega_m)}{\partial\omega_m} \int dS \Phi \nabla_n \Phi, \end{aligned} \quad (\text{B1})$$

where V_{met} and S are the volume and surface of metal nanoparticle, respectively, and ∇_n is the normal derivative. Using Eqs. (A3), we obtain

$$U_m = V_{\text{met}} \frac{\omega_m}{16\pi} \frac{\partial\varepsilon(\omega_m)}{\partial\omega_m} = ab^2 \frac{\omega_m}{12} \frac{\partial\varepsilon(\omega_m)}{\partial\omega_m}. \quad (\text{B2})$$

Appendix C: Plasmon radiative decay in spheroidal particles

The decay rate of a plasmon mode in metal-dielectric system has the form

$$\gamma_m^r = \frac{\omega_m^4}{3c^3} \frac{\mathcal{P}_m^2}{U_m} \quad (\text{C1})$$

where $\mathcal{P}_m = (4\pi)^{-1} \int dV \mathbf{E}_m(\mathbf{r}) [\varepsilon'(\omega_m, \mathbf{r}) - 1]$ is plasmon dipole moment. Due to the Gauss law, \mathcal{P}_m can be written as surface integral

$$\mathcal{P}_m = \frac{\varepsilon'(\omega_m) - 1}{4\pi} \int dS \Phi_m(\mathbf{s}) \mathbf{n}, \quad (\text{C2})$$

where \mathbf{n} is normal to the surface. For prolate spheroids, the potentials are given by Eq. (A2) and the normal vectors are simply $\mathbf{n} = \hat{\xi}$. Using the addition formula

$\hat{\xi} \cdot \hat{\xi}' = \cos\theta \cos\theta' + \sin\theta \sin\theta' \cos(\phi - \phi')$ for solid angle in spheroidal coordinates ($\eta = \cos\theta$), we obtain

$$\mathcal{P}_L^2 = \left[\frac{a^2 b}{3} [\varepsilon'(\omega_m) - 1] g_L(\xi_1) \right]^2, \quad (\text{C3})$$

where $\xi_1 = a/\sqrt{a^2 - b^2}$ and

$$g_L(\xi) = \frac{3\xi^3}{8} \arctan \frac{1}{\sqrt{\xi^2 - 1}} - \frac{3(\xi^2 - 2)}{8\xi} \sqrt{\xi^2 - 1}, \quad (\text{C4})$$

is a function that changes in the range $0.5 \div 1.0$, reaching the upper limit for sphere ($\xi \rightarrow \infty$). Using Eqs. (C3) and (B2), the plasmon radiative decay rate is evaluated as

$$\gamma_L^r = \frac{4\sqrt{\varepsilon_s} \omega_m^3 a^3 [\varepsilon'(\omega_m) - \varepsilon_s]^2}{9c^3} \frac{\partial\varepsilon'(\omega_m)/\partial\omega_m}{\partial\varepsilon'(\omega_m)/\partial\omega_m} g_L^2(\xi_1), \quad (\text{C5})$$

where we restored the dielectric constant of surrounding medium ε_s . Note that radiative decay rate for spheroidal particle scales as a^3 rather than as particle volume, implying high radiation efficiency for elongated particles.

For spherical particle ($a = b$), we have $g_L = 1$ and $\varepsilon'(\omega_{sp}) = -2$, and so the plasmon radiative decay rate (35) is recovered. The nanosphere polarizability (53) is recovered as well using $U_{sp} = a^3 \omega_{sp} [\partial\varepsilon'(\omega_{sp})/\partial\omega_{sp}]/12$ and $\mathcal{P}_{sp}^2 = a^6$, so that

$$\frac{\omega_{sp} \mathcal{P}_{sp}^2}{4U_{sp}} = \frac{3a^3}{\partial\varepsilon'(\omega_{sp})/\partial\omega_{sp}}. \quad (\text{C6})$$

For nanosphere in dielectric medium, right hand side of Eq. (C6) should be multiplied by ε_s .

Appendix D: Mode volume and Purcell factor for spheroidal particles

Using the Gauss law and expressing local fields in terms of potentials, the mode density projected along nanorod major axis takes the form

$$\rho_L(\mathbf{r}) = \frac{2}{\omega_m \partial\varepsilon'(\omega_m)/\partial\omega_m} \frac{[\nabla_n \Phi_m(\mathbf{r})]^2}{\int dS \Phi_m \nabla_n \Phi_m}, \quad (\text{D1})$$

where integration takes place over the metal surface. For \mathbf{r} at the distance d from the tip of a prolate spheroidal particle with major and minor semiaxes a and b , respectively, so that $\xi_1 = a/\sqrt{a^2 - b^2}$ at the surface, and using that $h_\xi = f$ along the z -axis, we obtain

$$\rho_L = \frac{1}{\mathcal{V}_L} = \frac{2}{V_{\text{met}} \omega_L} \left[\frac{\partial\varepsilon'(\omega_L)}{\partial\omega_L} \right]^{-1} \left[\frac{Q_1'(\xi) \xi_1}{Q_1(\xi_1)} \right]^2, \quad (\text{D2})$$

where $\xi = (a+d)/\sqrt{a^2 - b^2}$ and $V_{\text{met}} = 4\pi ab^2/3$ is the Au nanorod volume. The plasmon frequency ω_L follows from the boundary condition $\varepsilon'(\omega_L) = \varepsilon_s Q_1'(\xi_1) \xi_1 / Q_1(\xi_1)$. In

the limit of spherical particle of radius a , i.e., $f \rightarrow 0$ and $\xi \rightarrow \infty$ as $b \rightarrow a$, we have $Q(\xi) \approx 1/3\xi^2$, yielding

$$\rho_{\text{sph}} = \frac{1}{V_{\text{sph}}} = \frac{6}{\pi\omega_L} \left[\frac{\partial \varepsilon'(\omega_L)}{\partial \omega_L} \right]^{-1} \frac{a^3}{(a+d)^6}. \quad (\text{D3})$$

Note that for random dipole orientations, the orientational averaging results in the additional factor 1/3 in

Eqs. (D2) and (D3). Finally, the Purcell factor for QE at distance d from the nanorod tip is given by

$$F_p = \frac{12\pi\varepsilon_s Q_L}{k^3 V_{\text{met}} \omega_L \partial \varepsilon'(\omega_L) / \partial \omega_L} \left[\frac{Q'_1(\xi) \xi_1}{Q_1(\xi_1)} \right]^2, \quad (\text{D4})$$

and scales as $(k^3 V_{\text{met}})^{-1}$.

-
- [1] S. A. Maier and H. A. Atwater, *J. Appl. Phys.* **98**, 011101 (2005).
- [2] E. Ozbay, *Science* **311**, 189 (2006).
- [3] M. I. Stockman, in *Plasmonics: Theory and Applications*, edited by T. V. Shahbazyan and M. I. Stockman (Springer, New York, 2013).
- [4] E. C. Le Ru and P. G. Etchegoin, *Principles of Surface-Enhanced Raman Spectroscopy* (Elsevier, 2009).
- [5] E. Dulkeith, A. C. Morteaux, T. Niedereichholz, T. A. Klar, J. Feldmann, S. A. Levi, F. C. J. M. van Veggel, D. N. Reinhoudt, M. Moller, and D. I. Gittins, *Phys. Rev. Lett.* **89**, 203002 (2002).
- [6] O. Kulakovich, N. Strekal, A. Yaroshevich, S. Maskevich, S. Gaponenko, I. Nabiev, U. Woggon, and M. Artemyev, *Nano Lett.* **2**, 1449 (2002).
- [7] P. Anger, P. Bharadwaj, and L. Novotny, *Phys. Rev. Lett.* **96**, 113002 (2006).
- [8] S. Kühn, U. Hakanson, L. Rogobete, and V. Sandoghdar, *Phys. Rev. Lett.* **97**, 017402 (2006).
- [9] F. Tam, G. P. Goodrich, B. R. Johnson, and N. J. Halas, *Nano Lett.* **7**, 496 (2007).
- [10] R. Bardhan, N. K. Grady, J. R. Cole, A. Joshi, and N. J. Halas, *ACS Nano* **3**, 744 (2009).
- [11] T. Ming, L. Zhao, Z. Yang, H. Chen, L. Sun, J. Wang, and C. Yan, *Nano Lett.* **9**, 3896 (2009).
- [12] J. Bellessa, C. Bonnand, J. C. Plenet, and J. Mugnier, *Phys. Rev. Lett.* **93**, 036404 (2004).
- [13] Y. Sugawara, T. A. Kelf, J. J. Baumberg, M. E. Abdelsalam, and P. N. Bartlett, *Phys. Rev. Lett.* **97**, 266808 (2006).
- [14] G. A. Wurtz, P. R. Evans, W. Hendren, R. Atkinson, W. Dickson, R. J. Pollard, A. V. Zayats, W. Harrison, and C. Bower, *Nano Lett.* **7**, 1297 (2007).
- [15] N. T. Fofang, T.-H. Park, O. Neumann, N. A. Mirin, P. Nordlander, and N. J. Halas, *Nano Lett.* **8**, 3481 (2008).
- [16] T. K. Hakala, J. J. Toppari, A. Kuzyk, M. Pettersson, H. Tikkanen, H. Kunttu, and P. Torma, *Phys. Rev. Lett.* **103**, 053602 (2009).
- [17] D. E. Gomez, K. C. Vernon, P. Mulvaney, and T. J. Davis, *Nano Lett.* **10**, 274 (2010).
- [18] A. Manjavacas, F. J. Garcia de Abajo, and P. Nordlander, *Nano Lett.* **11**, 2318 (2011).
- [19] A. Berrier, R. Cools, C. Arnold, P. Oermans, M. Crego-Calama, S. H. Brongersma, and J. Gomez-Rivas, *ACS Nano* **5**, 6226 (2011).
- [20] A. Salomon, R. J. Gordon, Y. Prior, T. Seideman, and M. Sukharev, *Phys. Rev. Lett.* **109**, 073002 (2012).
- [21] S. Aberra Guebrou, C. Symonds, E. Homeyer, J. C. Plenet, Y. N. Gartstein, V. M. Agranovich, and J. Bellessa, *Phys. Rev. Lett.* **108**, 066401 (2012).
- [22] T. Antosiewicz, S. P. Apell, and T. Shegai, *ACS Photonics*, **1**, 454 (2014).
- [23] A. De Luca, R. Dhama, A. R. Rashed, C. Coutant, S. Ravaine, P. Barois, M. Infusino, and G. Strangi, *Appl. Phys. Lett.* **104**, 103103 (2014).
- [24] D. J. Bergman and M. I. Stockman, *Phys. Rev. Lett.*, **90**, 027402, (2003).
- [25] M. I. Stockman, *Nature Photon.* **2**, 327, (2008).
- [26] M. A. Noginov, G. Zhu, A. M. Belgrave, R. Bakker, V. M. Shalaev, E. E. Narimanov, S. Stout, E. Herz, T. Suteewong and U. Wiesner, *Nature*, **460**, 1110, (2009).
- [27] R. Carminati, J. J. Greffet, C. Henkel, J. M. Vigoureux, *Opt. Commun.* **261** 368 (2006).
- [28] J.-J. Greffet, M. Laroche, and F. Marquier, *Phys. Rev. Lett.* **105**, 117701 (2010).
- [29] C. Sauvan, J. P. Hugonin, I. S. Maksymov, and P. Lalanne, *Phys. Rev. Lett.* **110**, 237401 (2013).
- [30] R.-C. Ge, P. T. Kristensen, J. F. Young, and S. Hughes, *New J. Phys.* **16**, 113048 (2014).
- [31] X. Zambrana-Puyalto, and N. Bonod, *Phys. Rev. B* **91**, 195422 (2015).
- [32] A. E. Krasnok, A. P. Slobozhanyuk, C. R. Simovski, S. A. Tretyakov, A. N. Poddubny, A. E. Miroshnichenko, Y. S. Kivshar, and P. A. Belov, *Sci. Rep.* **5**, 12956 (2015).
- [33] G. C. des Francs, J. Barthes, A. Bouhelier, J. C. Weeber, A. Dereux, A. Cuche, and C. Girard, *J. Opt.* **18** 094005 (2016).
- [34] F. Marquier, C. Sauvan, and J.-J. Greffet, *ACS Phot.* **4**, 20912101 (2017).
- [35] A. F. Koenderink, *ACS Phot.* **4**, 710-722 (2017).
- [36] W. Yan, R. Faggiani, and P. Lalanne, *Phys. Rev. B* **97**, 205422 (2018).
- [37] L. Novotny and B. Hecht, *Principles of Nano-Optics* (CUP, New York, 2012).
- [38] E. M. Purcell, *Phys. Rev.* **69** (1946) 681.
- [39] S. Maier, *Opt. Express* **14**, 1957 (2006).
- [40] A. F. Koenderink, *Opt. Lett.* **35** 4208 (2010).
- [41] O. Di Stefano, N. Fina, S. Savasta, R. Girlanda, and M. Pieruccini, *J. Phys.: Condens. Matter* **22**, 315302 (2010).
- [42] F. Alpegiani, S. D'Agostino, and L. C. Andreani, *Phys. Rev. B* **86**, 035421 (2012).
- [43] P. T. Kristensen, C. Van Vlack, and S. Hughes, *Opt. Lett.* **37**, 1649 (2012).
- [44] P. T. Kristensen and S. Hughes, *ACS Phot.* **1**, 2 (2014).
- [45] E. A. Muljarov and W. Langbein, *Phys. Rev. B* **94**, 235438 (2016).
- [46] C. Sauvan, J. P. Hugonin, R. Carminati, and P. Lalanne, *Phys. Rev. A* **89**, 043825 (2014).
- [47] P. T. Kristensen, R.-C. Ge, and S. Hughes, *Phys. Rev. A* **92**, 053810 (2015).
- [48] P. Y. Chen, D. J. Bergman, Y. Sivan, arXiv:1711.00335.

- [49] P. Lalanne, W. Yan, K. Vynck, C. Sauvan, and J.P. Hugonin, *Laser Photon. Rev.* **12**, 1700113 (2018).
- [50] T. V. Shahbazyan, *Phys. Rev. Lett.* **117**, 207401 (2016).
- [51] L. D. Landau and E. M. Lifshitz, *Electrodynamics of Continuous Media* (Elsevier, Amsterdam, 2004).
- [52] W. Vogel and D.G. Welsch, *Quantum Optics* (Wiley, 2016).
- [53] A. N. Poddubny, I. V. Iorsh, and A. V. Sukhorukov, *Phys. Rev. Lett.* **117**, 123901 (2016) and Supplemental Material.
- [54] T. V. Shahbazyan, *Phys. Rev. B* **94**, 235431 (2016).
- [55] N. A. Mortensen, S. Raza, M. Wubs, T. Søndergaard, and S. I. Bozhevolnyi, *Nat. Commun.* **5**, 3809 (2014).
- [56] M. K. Dezfouli, C. Tserkezis, N. A. Mortensen, and S. Hughes, *Optica* **4**, 1503 (2017).